MIT Open Access Articles

Carbon nanotubes as piezoresistive microelectromechanical sensors: Theory and experiment

Citation	Cullinan, Michael A., and Martin L. Culpepper. "Carbon nanotubes as piezoresistive microelectromechanical sensors: Theory and experiment." Physical Review B 82.11 (2010): 115428. © 2010 The American Physical Society.
As Published	http://dx.doi.org/10.1103/PhysRevB.82.115428
Publisher	American Physical Society
Version	Final published version
Accessed	Mon Sep 24 17:20:20 EDT 2012
Citable Link	http://hdl.handle.net/1721.1/60855
Terms of Use	Article is made available in accordance with the publisher's policy and may be subject to US copyright law. Please refer to the publisher's site for terms of use.
Detailed Terms	

Carbon nanotubes as piezoresistive microelectromechanical sensors: Theory and experiment

Michael A. Cullinan and Martin L. Culpepper[*]

Department of Mechanical Engineering, Massachusetts Institute of Technology, Cambridge, Massachusetts 02139, USA

(Received 24 May 2010; revised manuscript received 18 August 2010; published 16 September 2010)

Carbon-nanotube (CNT) -based strain sensors have the potential to overcome some of the limitations in small-scale force/displacement sensing technologies due to their small size and high sensitivity to strain. A better understanding of the dominant and limiting causes of high strain sensitivity is needed to enable the design and manufacture of high-performance sensor systems. This paper presents the theoretical framework that makes it possible to predict the strain sensitivity of a carbon nanotube based on it chiral indices (n,m). This framework is extended to capture the behavior of sensors composed of multiple CNTs in a parallel resistor network. This framework has been used to predict that a parallel resistor network of more than 100 randomly selected CNTs should have a gauge factor of approximately 78.5 ± 0.4. This is within the experimental error of the measured gauge factor of 75 ± 5 for such CNT resistor networks.

I. INTRODUCTION

As mechanical devices move toward the nanoscale, smaller and more sensitive force and displacement sensors are required to measure/control their behavior. For example, multiaxis microscale and nanoscale sensors with nanometer displacement resolution and/or piconewton force resolution are needed in many biological, materials science, and nanomanufacturing applications. Unfortunately, these resolutions are difficult to achieve given the size, sensitivity, and fabrication limitations associated with existing small-scale sensing techniques. Carbon-nanotube (CNT) -based strain sensors are attractive as force/displacement sensors since they are not subject to the same limitations. However, CNT-based sensors cannot be realized in a practical way unless we are able to model and predict their performance in strain sensing systems.

The physics and fabrication of traditional Microelectromechanical Systems (MEMS) sensing technologies do not scale favorably with geometric downscaling. Therefore, the practical utility of traditional sensing technologies is limited at the microscale/nanoscale. For example, the resolution of capacitive sensors scales with sensor area, making fine resolution sensors too large for many microscale/nanoscale sensor systems. Similarly, interferometry becomes impractical at the microsclae/nanoscale because of the relatively large optics that are required. Fine resolution, silicon-based piezoresistive sensing techniques are easily fabricated within mesoscale devices but are difficult to realize in nanoscale devices due to limitations associated with photolithography and ion implantation.

The preceding fosters the need to identify technologies that are less problematic and advance their performance via new approaches. The dominant/limiting physics of CNT-based strain sensors do not preclude practical utility at the small scale. Nanoscale fabrication of CNT-based transducers is not limited by lithography/implantation since CNTs are inherently nanoscale materials. Also, CNTs have characteristics that yield increase performance/sensitivity. CNTs have been shown to have gauge factors in excess of 2900.[1] This is about an order or magnitude larger than silicon-based pi-ezoresistors. These properties make CNTs the optimal sensors for fine resolution microscale/nanoscale flexural transducers.

A better understanding of the link between applied strain and resistance is required in order to realize the potential of CNT-based transducers. This paper presents a theoretical model of CNT gauge factor that is based on tight-binding and zone-folding approximations. With this model, it is possible to (i) identify the types of CNTs that are most sensitive to strain and therefore best suited for use in high-resolution CNT-based flexural transducers, and (ii) evaluate the piezoresistance of CNT films.

II. PRIOR ART

Early experiments have showed that CNTs have the potential to be high-quality strain sensors. For example, Tombler *et al.*[2] used atomic force microscopy (AFM) tips to depress, and therefore strain, a suspended CNT. Using this method they showed that the conductance of a CNT may change by two orders of magnitude when strain is applied. Simulations showed that this result may have been the result of local deformations in the CNT structure around the AFM tip as opposed to uniform strain in the CNT.[3] However, later experiments that uniformly strained the entire CNT showed that CNT gauge factor could be as high as 2900.[1] Also, gauge factor has been shown to vary widely with the electrical structure of a CNT.[4–6] For example, Grow *et al.* showed that CNT gauge factor could be positive or negative.[6] Given the sensitivity and variability of gauge factor with structure, the creation of practical devices can only happen if one has the ability to specify the CNT that is best suited for a specific sensing application.

Theory and simulation have been used to predict the relationship between structure and gauge factor. These models and simulations are typically used to estimate the change in band gap between different types of CNTs. Gauge factor is then found by relating the band gap to CNT resistance. For example, Chen *et al.* showed that a 1% strain of a (12,0) CNT should result in a 6.4% decrease in resistance.[7] Yang *et al.*[8] used tight-binding models to show that CNT band gap
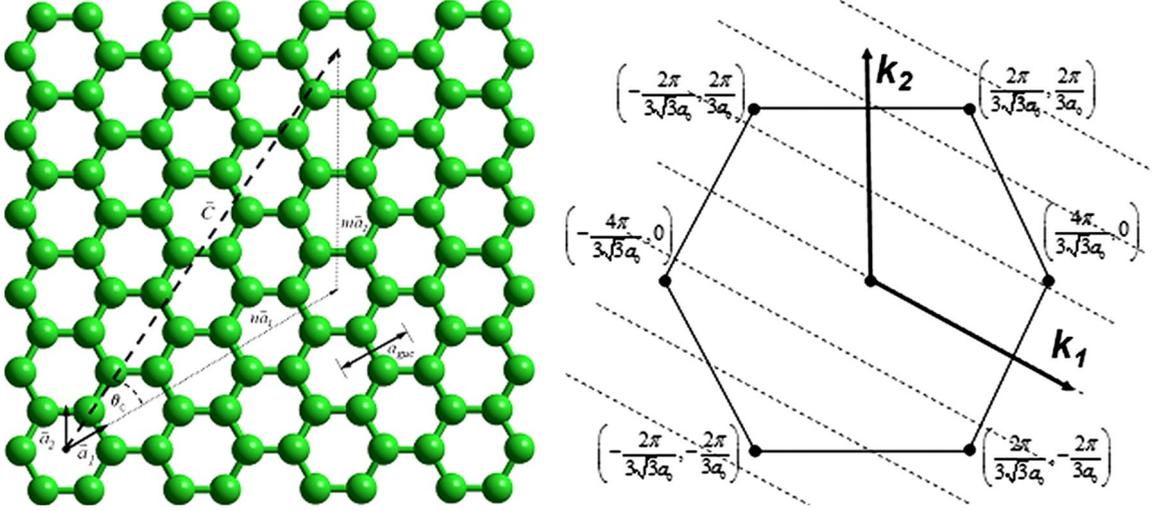
FIG. 1. (Color online) (a) CNT chiral vectors. (b) Graphene first Brillouin zone with allowed electronic states.

could increase or decrease depending on the chirality of the CNT. Unfortunately, little quantitative work has been used to link specific CNT geometries to gauge factors.

III. THEORETICAL MODEL

Our approach is based on the tight-binding model Mintmire and White[9] use to predict the electronic structure of an undeformed CNT near the Fermi level. Yang and Han[10] showed that this model could be extended to relate chiral angle and strain to the shift of the Fermi point, k_F, away from Brillouin-zone vertices. The CNT may be thought of as a graphene sheet rolled up into a cylinder along the lattice vectors $\boldsymbol{a}_1$ and $\boldsymbol{a}_2$ as shown in Fig. 1(a).

The electronic states near the Fermi point may be analyzed using the first Brillouin zone of graphene as defined by the reciprocal-lattice vectors $\boldsymbol{K}_1$ and $\boldsymbol{K}_2$. In an undeformed lattice, the Fermi points lie on the vertices of hexagonal Brillouin zone. The allowed electronic states, given by the Born–von Karman boundary condition, lie on parallel lines, $\boldsymbol{k}$, that are perpendicular to the lattice vector $\boldsymbol{C}$, as seen in Fig. 1(b). The variations in electronic states that are induced by strain may be found by measuring how the Fermi point moves with respect to the lines as strain is applied.

The Fermi point may be found by solving the tight-binding equation,

$$E(k_F) = \left| \sum \frac{t_0 r_0^2}{r_i^2} e^{ik \cdot \mathbf{R_i}} \right|, \tag{1}$$

where r_0 is the original bond length, r_i is the deformed bond length, t_0 is the tight-binding overlap integral, and $\boldsymbol{R_i}$ is the deformed bond vector. Yang *et al.*[8] solved this equation and showed that,

$$\Delta k_F r_0 = (1 + \nu)\varepsilon \cos 3\theta + \gamma \sin 3\theta \tag{2}$$

where ν is the Poisson's ratio, θ is the chiral angle, ε is the axial strain, and γ is the torsional strain. The dispersion relation of the deformed graphene may then be found by expanding $E(\boldsymbol{k})$ at $\boldsymbol{k}_F$,

$$E(\mathbf{k} - \mathbf{k_F}) = \pm \frac{3}{2} t_0 r_0 |\mathbf{k} - \mathbf{k_F}|. \tag{3}$$

When Eqs. (2) and (3) are combined, the change in band gap for small strains may be calculated as shown in Eq. (4). The sign of the band-gap change is determined by the chiral indices such that $p = -1$, 0, or 1 depending on the value of $\mathrm{mod}(n-m, 3)$,[10]

$$\Delta E_{gap} = \mathrm{sgn}(2p + 1)3t_0[(1 + \nu)\varepsilon \cos 3\theta + \gamma \sin 3\theta]. \tag{4}$$

This equation works well for semiconducting and armchair CNTs with diameters larger than 1 nm.[11] For smaller CNTs and for primarily metallic CNTs, curvature may play a large role in the gauge factor and therefore must be accounted for in the band-gap theory.[12,13] We use a similar, nearest-neighbor tight-binding approach that captures the intrinsic curvature of the CNT. For primarily metallic CNTs, Kleiner and Eggert[14] showed that

$$\Delta E_{gap} = -\mathrm{sgn}\left(\frac{t_0 a^2}{4d^2} - \frac{ab\sqrt{3}}{2} \right) \frac{ab\sqrt{3}}{2} \varepsilon \cos 3\theta, \tag{5}$$

where a is the length of the graphene lattice unit vector, d is the diameter of the CNT, and b is the change in the transfer integral with change in bond length.

The change in electrical resistance due to strain can be calculated based on band-gap changes. The resistance of a CNT can be accurately modeled by considering electron transport to occur by thermal activation.[5] This model is given in Eq. (6), where $|t|^2$ is the transmission probability of electrons with $|E - E_F| > E_{Gap}$ crossing the energy barrier, R_c is the contact resistance, h is plank's constant, e is the charge on an electron, k is Boltzman's constant, and T is temperature in degree kelvin,

$$R = R_c + \frac{1}{|t|^2} \frac{h}{8e^2} \left[1 + \exp\left(\frac{E_{Gap}^0 + \frac{dE_{Gap}}{d\varepsilon}\varepsilon}{kT} \right) \right]. \tag{6}$$

The zero strain band gap, E_{Gap}^0, is[15]
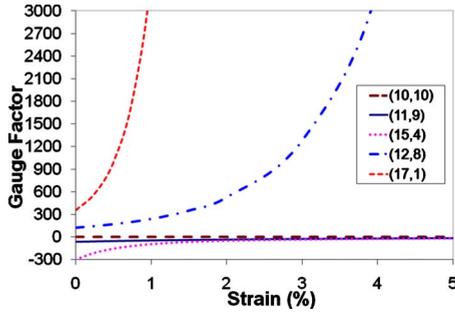
FIG. 2. (Color online) Gauge factor vs strain for CNTs with diameters of 1.38 nm.

$$E^0_{Gap} = \frac{2t_0 a}{\sqrt{3}d} \qquad (7)$$

for a semiconducting CNTs and[13]

$$E^0_{Gap} = \frac{t_0 a^2}{4d^2} \qquad (8)$$

for a metallic CNTs.

The gauge factor for any set of chiral indices may be calculated using Eqs. (6)–(8). Gauge factor for any material is defined by Eq. (9),

$$G_F \varepsilon = \frac{\Delta R}{R}. \qquad (9)$$

When Eq. (6) is substituted into Eq. (9), it can be shown that when $R_c \ll R$,

$$G_F = \frac{\dfrac{dE_{Gap}}{d\varepsilon}\exp\left(\dfrac{E^0_{Gap} + \dfrac{dE_{Gap}}{d\varepsilon}\varepsilon}{kT}\right)}{kT\left[\exp\left(\dfrac{E^0_{Gap} + \dfrac{dE_{Gap}}{d\varepsilon}\varepsilon_0}{kT}\right) + 1\right]}, \qquad (10)$$

where ε_0 is the pretension strain. Using this equation, the gauge factor for a specific CNT may be calculated by inserting Eqs. (4) and (7) for semiconducting CNTs, or Eqs. (5) and (8) for metallic CNTs, into Eq. (10).

IV. MODEL EVALUATION

Equation (10) predicts an exponential dependence of gauge factor on strain, which is consistent with observations.[1] From Eqs. (4)–(10), it may be seen that the (i) maximum magnitude of gauge factor occurs in zigzag $(n,0)$ CNTs and (ii) gauge factor decreases as the chiral angle increases, until a gauge factor of 0 for armchair CNTs (n,n). This trend, seen in Fig. 2, shows the behavior for five CNTs with diameters of $\sim$1.38 nm.

The CNTs in Fig. 2 show two distinct trends. The gauge factors of CNTs where $p=1$ are positive and increase toward infinity with increasing strain. This trend is consistent with the results observed by Stampfer et al.[1] The gauge factors of
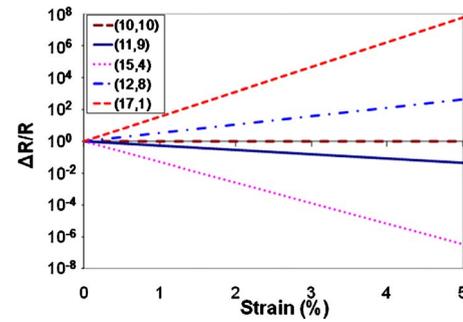
FIG. 3. (Color online) Resistance vs strain for CNTs with diameters of 1.38 nm.

the CNTs where $p=-1$ are negative and increase toward zero with increasing strain. This is consistent with results observed by Grow et al.[6] These two trends are the result of the exponential term in Eq. (10) where the sign of $dE_{Gap}/d\varepsilon$ determines whether the exponential increases toward infinity or approaches zero. Also, Fig. 2 shows that the (10,10) CNT has a gauge factor of 0 for all strains. This result is consistent with previously results for armchair CNTs.[16]

These trends may be better understood by examining how resistance changes with strain. From Fig. 3, it may be seen that the resistance of (17,1) and (12,8) CNTs increases exponentially with strain while the resistance of (15,4) and (11,9) CNTs decrease exponentially with strain. These trends give rise to the observed exponential dependence of gauge factor with strain as seen in Fig. 2. It is also important to note the magnitude of the slope of resistance vs strain in Fig. 3. The magnitude decreases as the chiral angle increases. This is responsible for the differences in gauge-factor sensitivity to strain that was shown in Fig. 2. In general, the constant gauge-factor approximation (i) holds over large strain ranges as the chiral angle increases and (ii) is more accurate for metallic CNTs than semiconducting CNTs with similar chiral angles.

Overall, near zero strain the maximum gauge factor for a semiconducting CNT is 362 while the maximum gauge-factor magnitude for a metallic CNT is 292. These values are much lower than the measured gauge factors reported by Stampfer et al.,[1] Cao et al.,[4] and Grow et al.[6] There are three likely explanations for these differences.

A small pretension on a CNT results in large increases in gauge factors when the CNT has a small chiral angle. Pretension could be induced during fabrication or within experimental setups. For example, the substrate the CNT is placed upon can induce a strain due to van der Waals interactions. Molecular mechanics simulations have estimated deformations as large as 2% for a (10,10) CNT.[17] This level of pretension would cause higher than expected gauge factors.

Another possibility is that previous experiments may have unknowingly measured the characteristics of CNT bundles rather than individual single walled carbon nanotubes (SWCNTs). The CNTs measured by Grow et al.[6] ranged from 2–6 nm in diameter, therefore it is likely that some of the larger diameter CNTS were bundles of smaller SWCNTs. Bundling reduces band gap of semiconducting CNTs, opens a secondary band gap in metallic CNTs, and changes electronic dispersion.[18]
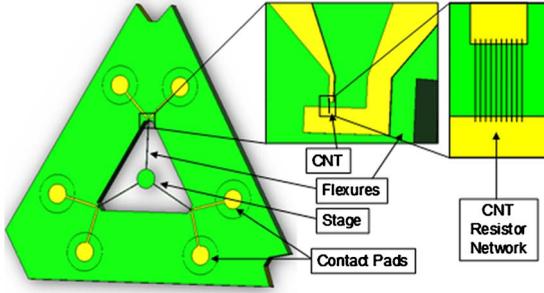
FIG. 4. (Color online) MEMS multiaxis force sensor with CNT-based strain sensors.

FIG. 5. (Color online) Resistance vs strain for a 100 CNT resistor network, with segregated contributions from metallic and semiconducting CNTs.

Some of the difference could be a result of effects that are not captured by the model. Increased electron scattering and changes in the Schottky barrier may also affect gauge factor, though at this point it is unclear how large the effect is.

Isolating the magnitude of error associated with the possible causes will require a larger study that links chiral indices to resistance and gauge factor at different temperatures. This is a rather involved study that will be taken up in the future. As will be seen in Sec. VI, our model matches experiments results for networks of CNTs with less than 7% error.

V. DESIGN OF A DEVICE THAT USES MANY CNTs IN PARALLEL FOR SENSING

The theory in Sec. III may be used to design devices with CNTs, for example the force sensor shown in Fig. 4. This sensor consists of three flexural beams that are used to measure out-of-plane forces and torque about an axis that is normal to the plane of the device and aligned with its axis of symmetry. In this design, several CNTs are placed in a parallel resistor network upon the flexure beams. When the beams strain, the CNTs strain, and this may be used to measure force and/or displacement.

The resolution of a strain sensor is set by sensitivity of the device output to strain (i.e., gauge factor) and noise. In CNT-based strain sensors, the dominate noise source is flicker noise.[19] Flicker noise is caused by the capture and release of charge carriers in localized trap states within the CNT.[20] The flicker noise in a CNT is given by Eq. (11), where α is the Hooge constant, V_s is the source voltage, f is the frequency, and N is the number of charge carriers in the resistor,

$$\sigma_{1/f} = \sqrt{\frac{\alpha V_s^2}{N} \ln\left(\frac{f_{max}}{f_{min}}\right)}. \tag{11}$$

From this equation, it is possible to decrease the flicker noise by increasing the number of charge carriers in the resistor. This may be accomplished, without reducing sensitivity, by replacing a single CNT sensor with a network of parallel CNTs.[21]

The feasibility of this design was investigated via a Monte Carlo simulation of a 100 CNT resistor network. In this simulation, the carbon nanotubes are modeled as independent resistors in parallel with equal amounts of strain applied to each CNT. The Monte Carlo simulation was run 10 000 times at strain intervals of 0.1% from 0% to 5% strain. Each
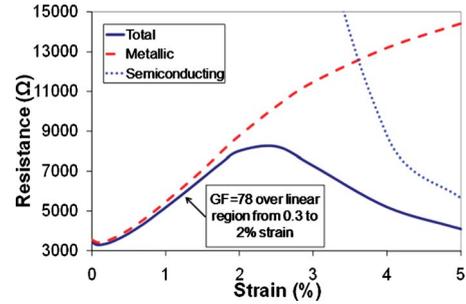
of the CNTs chiral indices was randomly selected from the pool of CNTs with diameters between 0.5 and 4 nm with each chiral index given equal weighting. The average resistance and gauge-factor results of these simulations at each strain level are presented in Figs. 5 and 6.

For small strains, the network resistance is dominated by the metallic CNTs because they have a lower resistance. Initially, the change in resistance is small and slightly negative. This is due to the closing of the secondary band gap in the metallic CNTs. At approximately 0.3% strain, the band gap in the metallic CNTs is zero and a new energy gap starts to open, thereby causing the band gap to increase. This results in the observed increase in resistance between 0.3% and 2% strain. Over this range, the change in resistance is close to linear with an R^2 of 0.997 and a gauge factor of 78.5 ± 0.4. This is close to the results reported in literature of 79 to 134 for aligned CNT films.[22] At 2.5% strain, the contributions from the semiconducting CNTs become significant and the resistance starts to decrease. In practice, most devices are likely to work within the linear regime between 0.3% and 2% strain due to the initial strain imposed on the CNT through interactions with the substrate or through other pretensioning effects.[17]

These resistance trends are the cause of the nonlinear gauge factor vs strain curves as seen in Fig. 6. The network gauge factor follows the metallic CNT behavior closely until approximately 2.5% strain. This is when the contributions from semiconducting CNTs become relevant. Initially, the semiconducting CNTs have a gauge factor of 0 because the $p=1$ CNTs increase in resistance with increasing strain while
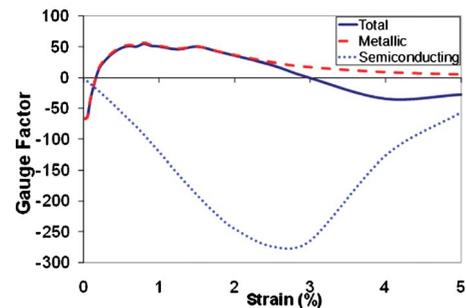
FIG. 6. (Color online) Gauge factor vs strain for a 100 CNT resistor network consisting of metallic, semiconducting, or all CNTs.

FIG. 7. (Color online) CNT parallel resistor network between two electrodes on the test structure.

the $p=-1$ CNTs decrease in resistance with increases in strain. These effects cancel out initially, but as strain increases, the behavior of the $p=-1$ CNTs start to dominate. This occurs because increasing strain causes more of the current in the network to be carried through the lower resistance, $p=-1$ CNTs. At high strains, the semiconducting CNTs act as $p=-1$ CNTs.

From Figs. 5 and 6, it is clear that the gauge factor of unsorted CNTs or CNTs sorted only into metallic and semiconducting CNTs is at least an order of magnitude smaller than for individual CNT sensors. A small number of $p=0$, $p=-1$ or other low gauge-factor CNTs can significantly reduce the sensitivity of the network. Therefore it is important to sort CNTs by chirality before constructing the networks if low noise and high strain sensitivity are desired.[23–26]

VI. EXPERIMENTAL PROCEDURE AND RESULTS

A MEMS test structure was designed and microfabricated, in order to test the predictions made in Secs. III–V. This test structure was incorporated into an experiment to measure the gauge factor of CNTs. As seen in Fig. 7, the test structure consists of a fixed-fixed flexure beam and electrodes connected to the base of the flexure. The outer four sets of electrodes are connected to polysilicon piezoresistors while the inner two electrodes are left empty so that CNTs may be connected across them. These central electrodes are spaced 1 μm apart. This architecture enabled us to measure the strain simultaneously and independently with the polysilicon and CNT piezoresistors. The center of the flexure has a locating hole where small, known weights may be placed, thereby loading the structure and straining the CNTs.

CNTs were deposited onto these test flexures via dielectrophoresis. A droplet of a 3 μg/mL solution of SWCNTs in deionized water was placed on the middle electrodes of the test structure and a 5 MHz, 5 V peak-to-peak ac voltage was used to direct the deposition of the SWCNTs. After 5 min, the test structure was rinsed with deionized water and dried. The results of this deposition process are shown in Fig. 8.

A low noise sensor system was connected in order to measure the gauge factor of the CNT network. The noise in the sensor electronics was more than an order of magnitude lower than the noise in the CNT sensor itself. The CNT network was incorporated into a dc Wheatstone bridge in a
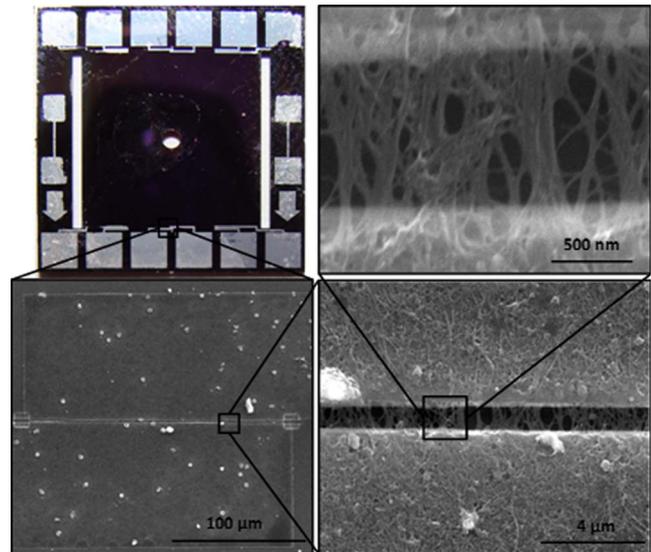
FIG. 8. (Color online) CNT resistor network between two electrodes on the test structure.

quarter bridge configuration. An instrumentation amplifier was used to boost the signal from the bridge, which is nulled with a bias voltage and read by an analog-to-digital converter.

Using this setup, the change in normalized resistance vs the change in strain was measured. The change in strain is used since the exact strain is unknown due to the pretension strain imposed on the CNT through its interaction with the SiO_2 substrate. Based on molecular mechanics simulations, this pretension strain is estimated to be approximately 1% for our setup.[17] The maximum change in strain that could be measured with this test setup was 0.1% due to fracture limit of the silicon beams. Using this test setup, the gauge factor of three different CNT resistor networks were measured as shown in Fig. 9. Each of these resistor networks was produced using the same dielectrophoresis process conditions described above. Sample 1 was measured to have a gauge factor of 73 ± 9 while samples 2 and 3 were measured to have gauge factors of 82 ± 9 and 70 ± 6, respectively. Overall, the average gauge factor of the three samples was calculated to be 75 ± 5. This result is within experimental error of
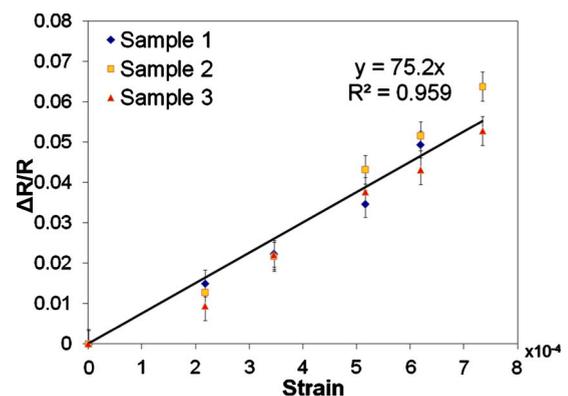
FIG. 9. (Color online) Measured change in resistance vs strain for CNT resistor networks.

the predicted value of 78.5 ± 0.4 that was presented in Sec. V. This indicates that the theory and models presented in Secs. III–V accurately capture the performance of CNT-based piezoresistors.

VII. CONCLUSION

CNT-based piezoresistors offer the potential to become versatile, high-resolution sensing systems. Existing CNT-based piezoresistive sensor systems are competitive with metal strain gauges in terms of performance. We have presented theory and a modeling approach that enables the prediction of gauge factor in general CNTs. The theoretical framework presented in this paper suggests the performance of CNT-based piezoresistive sensor systems could be improved by almost and order of magnitude if it becomes possible to accurately sort CNT by chirality.[23–26] This would allow CNT-based piezoresistive sensor systems to overcome many limitations presently found in microscale and nanoscale sensor systems.

This theoretical framework, which is based on tight-binding calculations for strained graphene sheets, also suggests that graphene sheets and nanoribbons could be used to produce high gauge-factor strain sensors. The primary difference in the theoretical analysis of carbon nanotubes and graphene sheets is that the band gap created by the curvature of the graphene sheet must be accounted for in the analysis of carbon nanotubes where as curvature does not have to be accounted for in the analysis of graphene sheets and nanoribbons. Also, in order to properly analyze the effects of strain on the electronic structure of graphene sheets and nanoribbons, the Born-von Karman boundary condition around the circumference of the carbon nanotube would need to be replaced by a particle in a particle-in-a-box like boundary condition. Both of these changes to the theoretical framework could have a major impact on the sensitivity of the strain sensing element. Therefore, more work needs to be done in this area to determine the ultimate viability of graphene sheets and nanoribbons as high-quality strain sensors.

---

*Corresponding author. FAX: 617 812 0384; culpepper@mit.edu

[1] C. Stampfer, A. Jungen, R. Linderman, D. Obergfell, S. Roth, and C. Hierold, Nano Lett. **6**, 1449 (2006).

[2] T. Tombler, C. Zhou, L. Alexseyev, J. Kong, H. Dai, L. Liu, C. S. Jayanthi, M. Tang, and S. Wu, Nature (London) **405**, 769 (2000).

[3] A. Maiti, A. Svizhenko, and M. P. Anantram, Phys. Rev. Lett. **88**, 126805 (2002).

[4] J. Cao, Q. Wang, and H. Dai, Phys. Rev. Lett. **90**, 157601 (2003).

[5] E. D. Minot, Y. Yaish, V. Sazonova, J. Y. Park, M. Brink, and P. L. McEuen, Phys. Rev. Lett. **90**, 156401 (2003).

[6] R. Grow, Q. Wang, J. Cao, D. Wang, and H. Dai, Appl. Phys. Lett. **86**, 093104 (2005).

[7] Y. Chen and C. Weng, Carbon **45**, 1636 (2007).

[8] L. Yang, M. P. Anantram, J. Han, and J. P. Lu, Phys. Rev. B **60**, 13874 (1999).

[9] J. W. Mintmire and C. T. White, Phys. Rev. Lett. **81**, 2506 (1998).

[10] L. Yang and J. Han, Phys. Rev. Lett. **85**, 154 (2000).

[11] R. Grow, in *Carbon Nanotubes: Properties and Applications*, edited by M. O'Connell (Taylor & Frances, New York, 2006).

[12] X. Blase, L. X. Benedict, E. L. Shirley, and S. G. Louie, Phys. Rev. Lett. **72**, 1878 (1994).

[13] S. Reich, C. Thomsen, and J. Maulsch, *Carbon Nanotubes: Ba-sic Concepts and Physical Properties* (Wiley-VCH, New York, 2004).

[14] A. Kleiner and S. Eggert, Phys. Rev. B **63**, 073408 (2001).

[15] R. Saito, G. Dresselhaus, and M. Dresselhaus, *Physical Properties of Carbon Nanotubes* (Imperial College, London, 2005).

[16] R. Heyd, A. Charlier, and E. McRae, Phys. Rev. B **55**, 6820 (1997).

[17] T. Hertel, R. E. Walkup, and P. Avouris, Phys. Rev. B **58**, 13870 (1998).

[18] S. Reich, C. Thomsen, and P. Ordejon, Phys. Rev. B **65**, 155411 (2002).

[19] P. Collins, M. Fuhrer, and A. Zettl, Appl. Phys. Lett. **76**, 894 (2000).

[20] S. Senturia, *Microsystem Design* (Springer, New York, 2001).

[21] J. Appenzeller, Y. Lin, J. Knoch, Z. Chen, and P. Avouris, IEEE Trans. NanoTechnol. **6**, 368 (2007).

[22] J. Tong and Y. Sun, IEEE Trans. NanoTechnol. **6**, 519 (2007).

[23] X. Tu, S. Manohar, A. Jagota, and M. Zheng, Nature (London) **460**, 250 (2009).

[24] L. Zhang, X. Tu, K. Welsher, X. Wang, M. Zheng, and H. Dai, J. Am. Chem. Soc. **131**, 2454 (2009).

[25] A. Nish, J. Hwang, J. Doig, and R. Nicholas, Nat. Nanotechnol. **2**, 640 (2007).

[26] X. Peng, N. Komatsu, T. Kimura, and A. Osuka, ACS Nano **2**, 2045 (2008).